materials

MDPI

Article

The Superconductivity in Bi-Doped $BaFe_2As_2$ Single Crystals

Jiabin Si [1,†], Jianfa Zhao [2,*,†], Ying Liu [1], Ying Liu [3], Changqing Jin [2], Jibing Liu [1] and Lingyi Xing [1,*]

[1] College of Physics and Electronic Science, Hubei Normal University, Huangshi 435002, China; s18639161575@163.com (J.S.); 18715482798@163.com (Y.L.); liujb@hbnu.edu.cn (J.L.)
[2] Beijing National Laboratory for Condensed Matter Physics, Institute of Physics, Chinese Academy of Sciences, Beijing 100190, China; jin@iphy.ac.cn
[3] Quantum Science Center of Guangdong-Hong Kong-Macao Greater Bay Area (Guangdong), Shenzhen 518045, China; liuying@quantumsc.cn
* Correspondence: zhaojf@iphy.ac.cn (J.Z.); xinglingyi@hbnu.edu.cn (L.X.)
† These authors contributed equally to this work.

Abstract: We have successfully synthesized a series of Bi-doped $BaFe_2As_2$ high-quality single crystals for the first time. X-ray diffraction (XRD) patterns show an expansion of lattice parameter *c* with Bi doping, indicating a negative pressure effect. By investigating the resistivity, a Fermi liquid (FL) to non-Fermi liquid (NFL) crossover is observed from normal state to antiferromagnetic order state, accompanied by three superconducting transitions labeled as SC I, SC II and SC III, which are supposed to be induced by three superconducting realms with various Bi concentrations. Thus, we propose that the NFL behavior is closely related to the presence of superconductivity. The magnetic susceptibility measurements further speculate that the SC I and SC III phases should exhibit filamentary superconductivity while the SC II exhibits a possible bulk superconductivity of T_C~7 K.

Keywords: $BaFe_2As_2$; iron-based superconductor; isovalent doping; negative pressure

check for updates

Citation: Si, J.; Zhao, J.; Liu, Y.; Liu, Y.; Jin, C.; Liu, J.; Xing, L. The Superconductivity in Bi-Doped $BaFe_2As_2$ Single Crystals. *Materials* **2024**, *17*, 929. https://doi.org/10.3390/ma17040929

Academic Editor: Andres Sotelo

Received: 22 January 2024
Revised: 9 February 2024
Accepted: 14 February 2024
Published: 17 February 2024

1. Introduction

Since the discovery of T_C = 26 K superconductivity in $LaO_{1-x}F_xFeAs$ [1], iron-based superconductors (IBSC) have stimulated another round of interest in high-temperature superconductor research regarding cuprates [2]. Among them, the '122' system $AEFe_2As_2$ (*AE* = Ba, Sr and Ca) with a $ThCr_2Si_2$-type structure has been heavily studied because of its easily grown, large, suitable and high-quality single crystals [3–5]. As for the $BaFe_2As_2$ parent compound [3], it exhibits an anomaly transition at 140 K which is attributed to a spin-density wave (SDW) and a tetragonal (*I*4/*mmm*) to orthorhombic (*Fmmm*) crystallographic structure transition. The superconductivity could eventually appear when the SDW transition is suppressed by applying physical pressure or chemical doping.

Compared with physical pressure, chemical doping has several alternative tuning modes, which can not only apply positive or negative chemical pressure but also introduce hole or electron carriers. For these reasons, it has been widely chosen as an effective method to investigate the superconductivity in $BaFe_2As_2$. For example, the superconductivity could be yielded by substituting isovalent P [6] or Ru [7] for As or Fe in order to introduce positive or negative chemical pressure, by substituting K for Ba to introduce hole carriers [3], and by substituting Co [8] or Ni [9] for Fe to introduce electron carriers. Unexpectedly, some other hole substitutions (Cr, Mn and V) at the Fe site could not induce superconductivity even though the SDW transition was also gradually suppressed [10–12]. The absence of hole carriers and a new competing *G*-type antiferromagnetic order has been proposed as a way to prevent the emergence of superconductivity in Mn- and Cr-doped $BaFe_2As_2$ [13,14]. However, even the strong hole-doping effect has been identified by Hall effect measurements in $Ba(Fe_{1-x}V_x)_2As_2$ [12], only local superconductivity along with coexisting magnetism is found to be consistent with the lack of bulk superconductivity [15]. This significant difference between hole doping and electron doping at the Fe site still

provokes debate. Moreover, another much simpler correlation mechanism is proposed in a review article that suggests a decrease in *c*-lattice parameter is required to induce 'in-plane' (FeAs layer) superconductivity [16]. Based on this guideline, the bulk superconductivity induced by electron dopants at the Fe site and isovalent dopant at the As site with a smaller P element seems to be easily understood. Even for the isovalent Ru doping at the Fe site can be well interpreted, although the radius of the Ru ion is larger than the Fe ion, since it only expands lattice parameter *a* and the volume but indeed causes a decrease in lattice parameter *c* [7].

Recently, Jayalakshmi et al. theoretically proposed that the superconductivity is possible in (Ca,Sr,Ba)Fe_2Bi_2 compounds and $BaFe_2Bi_2$ might exhibit a higher T_C (≈30 K) than other proposed materials [17,18]. However, the structural data show that lattice parameter *c* is larger than $BaFe_2As_2$, which is contrary to the previous prediction that *c* should be reduced for 'in-plane' bulk superconductivity. Further work must be performed in order to verify whether $BaFe_2As_2$ could become a superconductor by using isovalent Bi as a substitution for As to introduce a negative pressure and whether the relationship between the *c* decrease and bulk superconductivity is still satisfactory. In this work, we report the synthesis and investigation of Bi-doped $BaFe_2As_2$ single crystals experimentally for the first time. Two filamentary superconducting phases with T_C~25 K (SC I) and 15 K (SC III), and another possible bulk superconducting phase (SC II) with T_C~7 K, are found, which indirectly confirms the possible superconductivity of $BaFe_2Bi_2$; however, the reduction in lattice parameter *c* for 'in-plane' bulk superconductivity might be not sufficient.

2. Materials and Methods

The $BaFe_2(As_{1-x}Bi_x)_2$ single crystals were synthesized by self-flux method. $FeAs_{1-x}Bi_x$ were prepared as precursors using the highly pure raw materials Fe, As and Bi by solid reaction method. The Fe, As and Bi powders were thoroughly mixed together and sealed in an evacuated quartz tube. The mixture was heated up to 750 °C and kept for 30 h. The obtained material was reground and sintered twice using the same heating procedure in order to make the Bi doping much more homogeneous. After we obtained the precursors, the Ba lump, as well as the FeAs and $FeAs_{1-x}Bi_x$ powders, were loaded in the alumina oxide tube and sealed in the evacuated quartz tube according to the stoichiometry ratio 1:2:2. The quartz tube was heated up to 1150 °C for 20 h and then slowly cooled down to 1000 °C with a rate of 2 °C/h in order to grow single crystals. In the end, the high-quality single crystals with dimensions up to 8 mm × 6 mm × 0.1 mm were obtained, as shown in Figure 1a. All the synthesis manipulations were carried out in a glove box filled with high-purity nitrogen gas.

The surface morphology and actual chemical compositions of $BaFe_2(As_{1-x}Bi_x)_2$ single crystals were examined by a scanning electron microscope (SEM) equipped with energy dispersive X-ray spectroscopy (EDX). The X-ray diffraction (XRD) was conducted with 2θ range from 10° to 80° on a Rigaku X-ray diffractometer (SmartLab SE, Tokyo, Japan) using Cu K_α radiation (λ = 1.5406 Å) generated at 40 kV and 30 mA. Both the resistivity and DC magnetic susceptibility was measured by the Quantum Design's Magnetic Property Measurement System (MPMS3, San Diego, CA, USA). The resistivity was measured using the standard four-probe method, while the DC magnetic susceptibility was measured using the zero-field-cooling (ZFC) and field-cooling (FC) modes with two fields *H* = 20 Oe and 1 T along the *ab* plane.

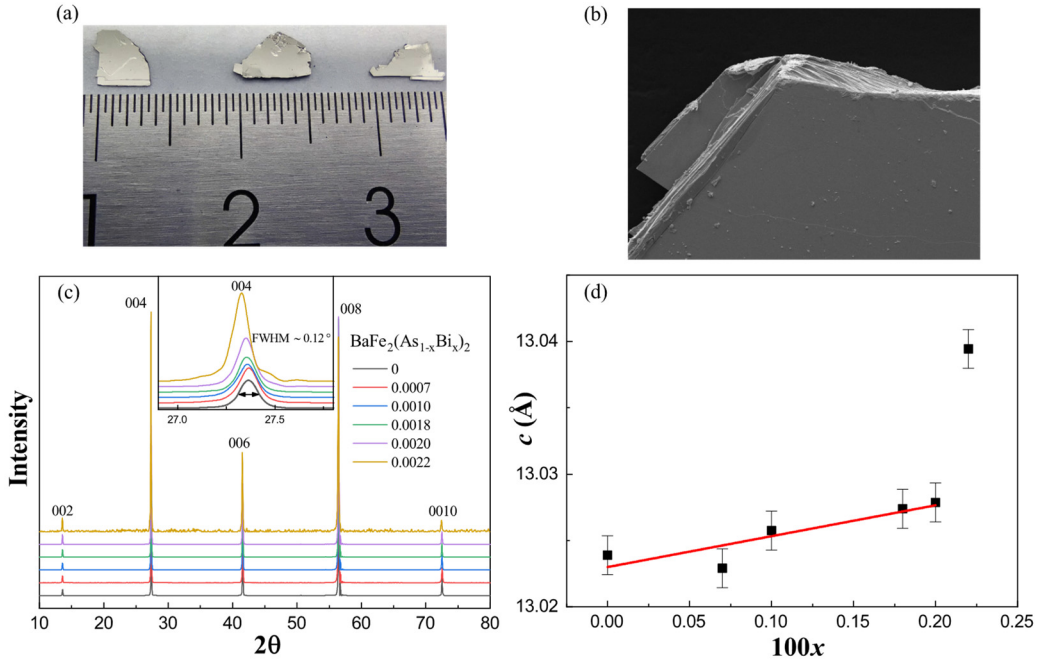

Figure 1. (**a**) The typical photograph, (**b**) the typical SEM surface morphology photograph, (**c**) the XRD patterns (inset is the enlarged (004) peaks and the FWHM is labeled) and (**d**) the concentration $100x$ dependence of lattice parameter c for $BaFe_2(As_{1-x}Bi_x)_2$ single crystals.

3. Results and Discussion

3.1. Actual Doping Concentration and Lattice Parameter c

We have successfully grown five batches of $BaFe_2(As_{1-x}Bi_x)_2$ single crystals for the first time. The typical photograph of the single crystals in Figure 1a shows a quite shiny and flat surface, and the surface morphology in Figure 1b taken by SEM clearly displays its layered structure; both reflect the high quality of our single crystals. In order to determine the actual Bi doping concentration, we conducted the EDX measurement. The single crystals were first cleaved in order to present a shiny surface. Then, three different regions were chosen to detect the concentration for each sample. Since the Bi-doping level was quite low, it was not homogeneous, which is also compatible with our later-proposed scenario in which there may exist three different realms in our sample (R I, R II and R III). Therefore, we took the averaged concentration as the actual concentration. The nominal and actual Bi concentration x are listed in Table 1, and the actual doping concentration x will be used to label the single crystals hereafter. We can find that the actual concentration of Bi is quite a bit lower than the nominal value and, with the increase in the nominal doping level, the actual concentration first increases slightly, but further decreases when nominal x is above 0.2. The highest actual doping level could only reach up to 0.22%. This indicates that it is quite difficult to dope the Bi into the As site, which may be a result of the solid solubility limit or an unstable phase.

Table 1. The nominal and actual doping concentration of $BaFe_2(As_{1-x}Bi_x)_2$ single crystals.

Nominal x	Actual x
0.01	0.0007
0.05	0.0020
0.10	0.0018
0.20	0.0022
0.35	0.0010

Figure 1c shows the XRD patterns of $BaFe_2(As_{1-x}Bi_x)_2$ single crystals. Only sharp $(00l)$ peaks can be reflected on the patterns, suggesting that the cleaved planes are perpendicular

to the *c*-axis. The inset is the enlarged (004) peaks. The high intensity and the narrow full width at half maximum (FWHM) labeled in the inset (2θ~0.12°) again indicate the high quality of our single crystals. Meanwhile, the (004) peak shifts to the lower diffraction angle with the increase in Bi concentration x, indicating that the Bi element is indeed introduced into $BaFe_2As_2$. The lattice parameter c for each doping sample was calculated using the XRD patterns and was plotted as a function of concentration $100x$ in Figure 1d. When x is below 0.002, the lattice parameter c increases almost linearly with the doping evolution, which is consistent with Vegard's law [19], and it begin to deviate above 0.002 with a step increase in lattice parameter c for the x = 0.0022 sample. Compared with P dopant, Bi substitution for As expands the *c*-axis, presenting a negative pressure effect which also matches the expectation since the radius of the Bi ion is larger than that of the As ion.

3.2. Superconducting Transitions and Non-Fermi Liquid Behavior

In order to investigate the superconducting properties, we first conducted resistivity measurements. Figure 2a displays the temperature dependence of resistivity down to 5 K measured with a 10 mA current for $BaFe_2(As_{1-x}Bi_x)_2$ single crystals. For all the samples, compared with the parent compound, a similar SDW transition around 135 K is found. But when temperature decreases to around 25 K, another transition happens with a drop of resistivity which may be associated with a superconducting transition. Actually, this kind of phenomenon is also observed in some $BaFe_2As_2$ [20,21], $CaFe_2As_2$ [22] and $SrFe_2As_2$ [23] parent compounds, as well as Ni-doped $BaFe_2As_2$ [24] and Pr-doped $CaFe_2As_2$ [25], which are proposed as filamentary superconducting transitions. For the x = 0.0022 sample, the percentage of resistivity dropping is highest: about 78%. Thus, we measured it again with lower 1 mA current and temperature down to 2 K, as shown in Figure 2c. Then, the zero resistivity was detected and, with the increase in the magnetic field, the transition temperature was suppressed gradually, confirming its superconducting properties. This significant dependence of resistivity on current is consistent with a more filamentary-natured superconductivity. To determine the antiferromagnetic (T_N) and superconducting (T_C) transitions, the temperature dependence of $d^2\rho/dT^2$ is plotted in Figure 2b and the minimum of $d^2\rho/dT^2$ is taken as the transition temperature marked by arrows. To our surprise, for the superconducting transition at low temperature, except for the one around 25 K (labeled as T_{C1}), there seem to have been another two superconducting transitions around 15 K (labeled as T_{C3}) and 10 K (labeled as T_{C2}). These transitions are much clearer for the x = 0.0022 sample under 1 mA, which can also be identified easily by the naked eye, as marked by arrows in Figure 2c. Corresponding with the three temperatures, three superconducting phases are defined as SC I (T_{C1}), SC II (T_{C2}) and SC III (T_{C3}).

The filamentary superconductivity (FL SC) has been argued to be attributed to the lattice distortion or strain [23], spin and orbital fluctuations [21], the antiphase domain walls [22] and the spontaneous electronic inhomogeneity at the nanoscale level [25]. Considering the average Bi concentration is quite low in our single crystals, we proposed our own scenario to interpret this behavior. We speculate that there might exist three kinds of realms in our sample: some realms (R I) are almost the same as the conditions found in the parent compound without any Bi dopants; some realms (R II) are highly Bi-doped; and the ratio of Bi doping in the rest of the realms (R III) is between the first two realms. The SC I with T_{C1}, the SC II with T_{C2}, and the SC III with T_{C3} originate from R I, R II and R III, respectively. The reasonable relationship between them will be discussed in detail later.

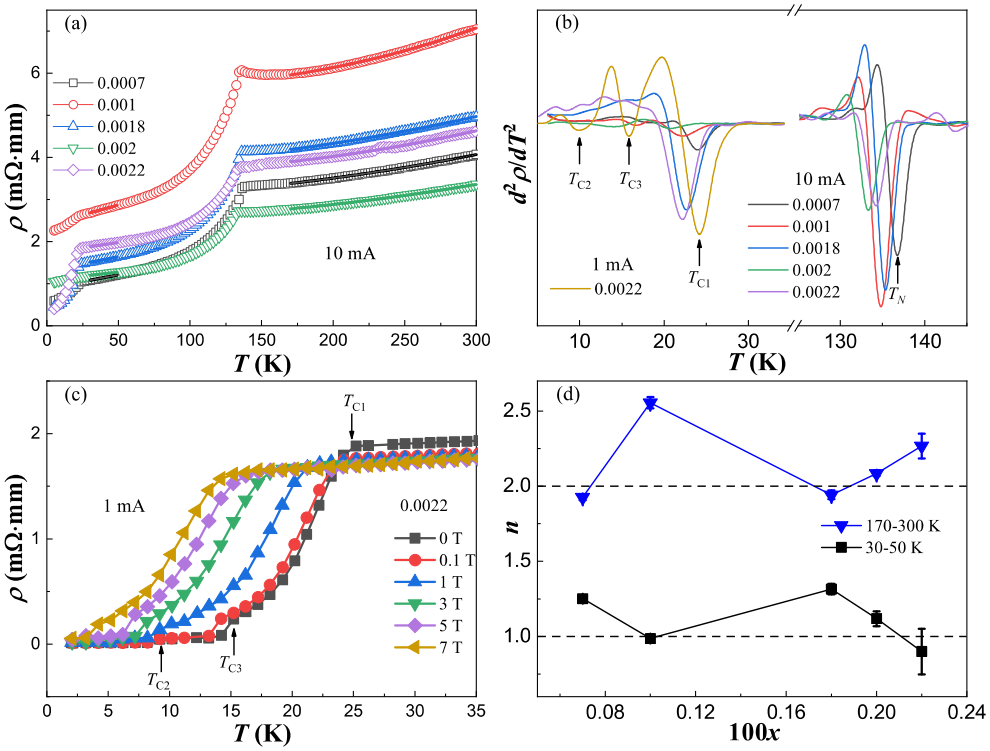

Figure 2. (**a**) The temperature dependence of resistivity measured with a 10 mA current for $BaFe_2(As_{1-x}Bi_x)_2$ single crystals. The solid lines are the fitting lines using the power law formula $\rho = \rho_0 + AT^n$ between 30 K and 50 K, and between 170 K and 300 K. (**b**) The $d^2\rho/dT^2$ as a function of temperature according to the data from (**a**,**c**). (**c**) The temperature dependence of resistivity under different magnetic fields measured with a 1 mA current for the $x = 0.0022$ sample. (**d**) The concentration $100x$ dependence of fitting parameter n obtained from (**a**).

In iron pnictides, the normal state of resistivity has been extensively described by the power law formula $\rho = \rho_0 + AT^n$, where n is the temperature exponent, ρ_0 is the residual resistivity, and A is a constant. Here, to avoid the antiferromagnetic (AFM) and superconducting transitions' influence, the 30–50 K (above T_{C1} and below T_N) and 170–300 K (above T_N) ranges are chosen as two fitting regions. The solid lines shown in Figure 2a represent the perfect fitting results using the power law. The evolution of n with Bi doping is summarized in Figure 2d. There is no significant doping dependence of n for both regions. However, n is much closer to 2 above T_N, thus corresponding to a Fermi-liquid (FL) ground state, while n is closer to 1 below T_N before the emergence of superconductivity, thus corresponding to a non-Fermi-liquid (NFL) behavior. This anomalous NFL behavior has often been revealed just above the superconducting dome, which may be closely tied to superconductivity [26,27]. Moreover, a simultaneous disappearance of the superconductivity and the NFL transport is observed in $CaFe_2(As_{1-x}P_x)_2$ [28]. From our results, this explicit indication of a FL to NFL crossover from normal state to AFM order state confirms the idea that NFL behavior may play a crucial role in the presence of superconductivity.

3.3. Superconducting Volume and Effective Moment

To further investigate the superconducting diamagnetism, the temperature dependence of magnetic susceptibility was measured using an $H = 20$ Oe magnetic field by the zero-field-cooling (ZFC) and field-cooling (FC) modes, as shown in Figure 3a–c. In contrast with the three superconducting transitions observed in resistivity, the one at T_{C1} could no longer be detected, while the one at T_{C3} was only detected in the low Bi-doping single crystals with $x = 0.0007$, 0.0010 and 0.0018 at 17 K, as shown in Figure 3a; the one at T_{C2} was only detected in the high Bi-doping single crystals with $x = 0.0020$ and 0.0022 at 7 K, as shown in Figure 3b. The absence of SC I in the magnetic susceptibility confirms its

filamentary-natured superconductivity. Although the SC III is present, the superconducting transition is broad and the shielding signal magnitude is very weak, so that only the x = 0.0018 sample shows a diamagnetic property below 6 K, indicating a very small superconducting volume fraction. The absolute superconducting volume (SC V) is calculated by $4\pi\chi_v(T_C) - 4\pi\chi_v(5\ K)$, as shown in Figure 5a (left axis). The SC V for x = 0.0007, 0.0010 and 0.0018 is about 0.01%, 0.01% and 0.09%, respectively. This indicates that the SC III is not a bulk superconductor, but it does reflect that the superconductivity is less filamentary compared with SC I, and the SC V increases with the increase in Bi doping. Especially with the further increase in Bi concentration, a very sharp superconducting transition and a dramatically enhanced shielding signal are observed for SC II, as shown in Figure 3b. The SC V for x = 0.0020 and 0.0022 has increased significantly: up to about 1.65% and 0.34%. With the increase in Bi doping, the SC V changes by order of magnitude, crossing from 0 for SC I to 10^{-2} order for SC III and then to 10^{-1} or 1 order for SC II. Since the chemical substitution can create local, hence average, structural changes which would then greatly impact the electronic structure, the lattice effect of Bi doping could not be ignored. This suggests that these three superconducting phases and doping levels are mutually related. Therefore, the scenario we proposed previously regarding the relationship between the three superconducting phases (SC I, SC II and SC III) and the three realms (R I, R II and R III) has been shown to be reasonable and easily understood. This can also be reflected by the disappearance of the SC I and SC II for x = 0.0007, 0.0010 and 0.0018, as shown in Figure 3a. Although both of them are invisible, the reasons are different. For SC I, it is the result of its filamentary nature's superconductivity property, which is related to the realm with almost no Bi doping, but for SC II, it is highly related to the Bi-doping level and its disappearance is attributed to the lack of Bi concentration. Moreover, compared with the SC V for x = 0.0007, the relative variation ratio $(V - V(x = 0.0007))/V(x = 0.0007)$ is also plotted as a function of $100x$, as shown in Figure 5a (right axis). Even though all of our single crystals show a non-bulk superconductivity with SC V, less than 2%, the relative variation ratio has a dramatic increase, up to 600%, 13,300% and 2565% for x = 0.0018, 0.0020 and 0.0022, respectively, clearly heralding the emergence of a possible bulk superconductivity (Bulk SC) for SC II. The reason why the bulk superconductivity was not shown in our sample is that the actual Bi concentration is still too low. We wonder if a true bulk superconductor could have emerged if the Bi concentration had been further increased. This idea is also supported by the theoretical calculation that the parent $BaFe_2Bi_2$ might hold T_C~30 K superconductivity [18].

To study the upper critical field $\mu_0 H_{C2}$, the magnetic susceptibility for x = 0.0022 was measured again, down to 2 K, under various magnetic fields, up to 700 Oe, as shown in Figure 3c. As the field increases, the superconducting transition is gradually suppressed to a lower temperature, confirming its superconductivity properties. Combined with the resistivity and magnetic susceptibility, by taking the data from Figures 2c and 3c, the T_C value at each field is plotted as $\mu_0 H_{C2}$ versus T, as shown in Figure 3d. The dashed curves are fits to the Werthamer–Helfand–Hohenberg (WHH) relation [29], $H_{C2}(0) = -0.693 T_C (dH_{C2}/dT)_{T=Tc}$, and the solid curves are fits to Ginzburg–Landau (GL) model: $H_{C2}(T) = H_{C2}(0)\ [(1 - t^2)/(1 + t^2)]$, where t represents the normalized temperature T/T_C. The obtained fitting parameters of T_C and $\mu_0 H_{C2}$ are summarized in Table 2. The values of T_C are consistent with each other while the values of $\mu_0 H_{C2}(0)$ obtained from WHH are lower than GL, which is similar to those reported in other iron pnictide superconductors [30,31]. These values are much smaller than the nominal Pauli paramagnetic limit, which is roughly estimated by $\mu_0 H^P = 1.84 T_C$ [32], indicating the orbital limit effect. The GL coherence length ξ_{GL}, shown in Table 2, is also calculated using the relation $\mu_0 H_{C2}(0) = \Phi_0/(2\pi\xi_{GL}^2)$, where $\Phi_0 = 2.07 \times 10^{-15}$ T·m^2 is the flux quantum.

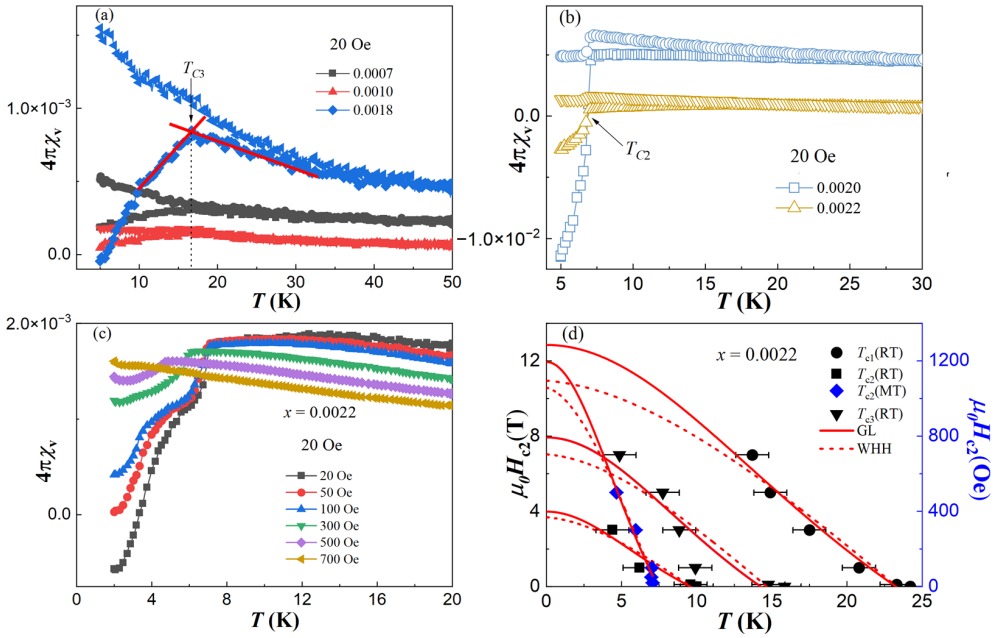

Figure 3. The temperature dependence of magnetic susceptibility for (**a**) $BaFe_2(As_{1-x}Bi_x)_2$ (x = 0.0007, 0.0010 and 0.0018) with H = 20 Oe magnetic field, (**b**) x = 0.0020 and 0.0022 with H = 20 Oe magnetic field, and (**c**) x = 0.0022 under different magnetic fields. (**d**) The temperature dependence of $\mu_0 H_{c2}$ for x = 0.0022 sample. The black points corresponding to the left coordinate axis are obtained from resistivity data in Figure 2c, and the blue points corresponding to the right coordinate axis are from the magnetization data in (**c**). The red solid lines are the fitting lines according to GL function, and the red dash lines are according to WHH function.

Table 2. The superconducting transition temperature T_C, upper critical field $\mu_0 H_{C2}$ and GL coherence length ξ_{GL} parameters obtained from WHH and GL fits for the three superconducting phases derived from resistivity and magnetic susceptibility measurements for the x = 0.0022 sample.

x = 0.0022	WHH Fit		GL Fit		
	T_C (K)	$\mu_0 H_{C2}$ (T)	T_C (K)	$\mu_0 H_{C2}$ (T)	ξ_{GL} (Å)
SC I (RT)	23.3	10.91	23.2	12.90	51
SC II (RT)	9.6	3.67	9.6	3.98	91
SC II (MT)	7.3	0.11	7.4	0.12	524
SC III (RT)	14.7	7.01	14.3	7.93	65

Magnetic susceptibility is also measured by applying the H = 1 T magnetic field, as shown in Figure 4a. The SDW transitions are observed for all the single crystals and the minimum of $d^2\chi/dT^2$ plotted in Figure 4b is taken as the AFM transition temperature, which is consistent with the resistivity measurement. Above T_N, the magnetic susceptibility shows a T-linear behavior for x = 0.0007 and 0.0010, which is universal in iron pnictides and is explained by the existence of a wide antiferromagnetic fluctuation [33]. When x > 0.0018, the deviation from T-linear behavior becomes obvious and gradually changes to a Curie–Weiss-like behavior. As shown in Figure 4c, the magnetic susceptibilities can be well fitted between 150 K and 220 K by the Curie–Weiss law $1/(\chi - \chi_0) = (T - \theta_{CW})/C$, where χ_0 is the temperature-independent magnetic susceptibility, θ_{CW} is the Curie temperature and C is the Curie–Weiss constant. The extracted effective moment μ_{eff} per Fe is plotted in Figure 4d. The values are about 1.95μ_B, 2.26μ_B and 1.74μ_B for x = 0.0018, 0.0020 and 0.0022, corresponding to an effective spin close to S = ½, and comparable with a value of about 1.9μ_B for the parent compound $BaFe_2As_2$, as studied by inelastic neutron scattering [34]. It seems that the effective moment is almost independent from the Bi substitution. In contrast,

the effective moment gradually decreases with increasing x for the other two isovalent substitution systems in $BaFe_2(As_{1-x}P_x)_2$ [35,36] and $Ba(Fe_{1-x}Ru_x)_2As_2$ [37,38]. Especially for the $Ba(Fe_{1-x}Ru_x)_2As_2$ system, Ru substitution also presents a negative pressure effect, but with a decrease in the c-axis. The dilution of the magnetic moment at the Fe site is contributed to a decrease in z_{As}, which is correlated with a decrease in the c-axis [38]. Therefore, the doping independence of effective moment in our $BaFe_2(As_{1-x}Bi_x)_2$ sample may be linked to the increase in the c-axis.

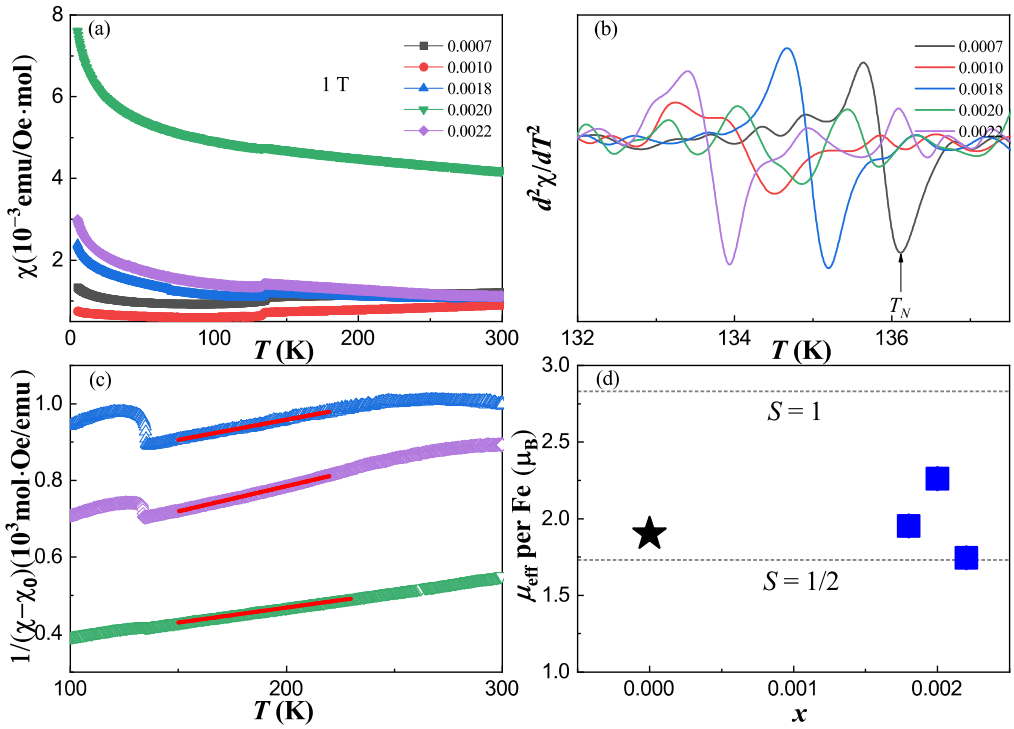

Figure 4. (**a**) The temperature dependence of magnetic susceptibility for $BaFe_2(As_{1-x}Bi_x)_2$ single crystals with H = 1 T magnetic field. (**b**) The $d^2\chi/dT^2$ as a function of temperature according to the data from (**a**). (**c**) The temperature dependence of $1/(\chi - \chi_0)$ for x = 0.0018, 0.0020 and 0.0022 samples. The red solid lines are fits to the Curie–Weiss law. (**d**) The effective moment per Fe site as a function of the doping concentration x. The blue square points are our results, and the black star point is from reference [34].

3.4. Superconducting Phase Diagram

Based on the resistivity and magnetic susceptibility data, we constructed a complete temperature-doping phase diagram of $BaFe_2(As_{1-x}Bi_x)_2$ which is presented in Figure 5b. One AFM phase and three superconducting phases labeled as SC I, SC II and SC III are well defined and coexistent. The T_C is about 25 K, 15 K and 7 K for SC I, SC III and SC II, respectively. Attributed to the relatively low Bi concentration, the coexistence of the AFM state and superconductivity might only occur in the microscopic region. In addition, both the AFM and superconducting transition temperatures seem to be independent from the slight Bi variation. From the normal state to the AFM order state, a FL to NFL crossover is revealed and the NFL behavior appears right at the boundary of superconducting phases, which may be a significant factor driving the presence of superconductivity. The red data points in the superconducting region demonstrate that only the SC II and SC III could be detected by the diamagnetic signal. Combined with the dramatic enhancement of SC V in Figure 5a, we strongly suggest that these superconducting phases are closely correlated with the Bi concentration; the SC I and SC III should be filamentary superconductors, while the SC II should be a bulk superconductor.

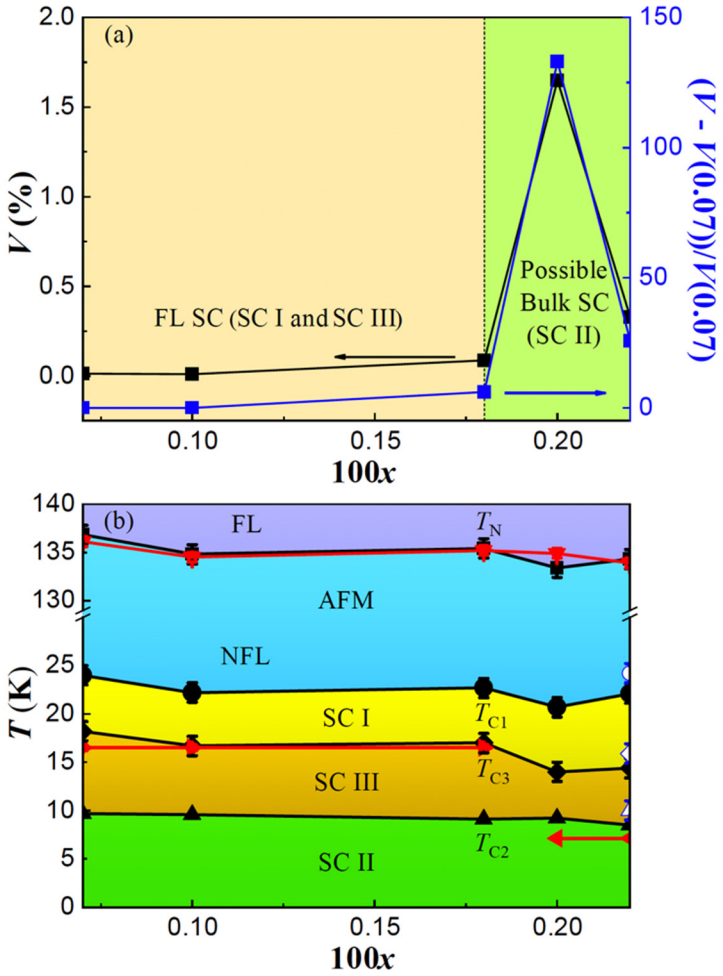

Figure 5. (**a**) The concentration $100x$ dependence of superconducting volume (left axis) and the relative variation ratio $(V - V(x = 0.0007))/V(x = 0.0007)$ (right axis). (**b**) The phase diagram of $BaFe_2(As_{1-x}Bi_x)_2$ as a function of concentration $100x$. The solid black (empty blue) points are derived from resistivity measured with 10 mA (1 mA) current. The solid red points are derived from magnetic susceptibility.

4. Conclusions

In conclusion, a series of high-quality $BaFe_2(As_{1-x}Bi_x)_2$ single crystals were successfully grown for the first time. The highest doping level could only reach up to 0.22%, and the Bi doping enlarged lattice parameter c, showing a negative pressure effect. By investigating resistivity and magnetic susceptibility, a FL to NFL crossover from normal state to AFM state, and three superconducting phases labeled as SC I, SC II and SC III, were observed. We assume that the NFL behavior plays a crucial role in the presence of superconductivity. The evolution of SC V with Bi doping suggests that these superconducting phases should be highly related to the Bi doping concentration, and the SC II with T_C~7 K is proposed as a possible bulk superconductor. Thus, the previous prediction regarding the superconductivity in parent $BaFe_2Bi_2$ is possible, and the reduction in lattice parameter c for 'in-plane' bulk superconductivity might be not sufficient. To further confirm our scenarios regarding the origin of the three superconducting phases, we recommend that scanning tunneling microscopy measurements be conducted for specific investigation in the future.

Author Contributions: Conceptualization and supervision, L.X.; investigation, J.S., J.Z., Y.L. (Ying Liu 1), C.J., J.L. and Y.L. (Ying Liu 2); formal analysis and writing—original draft preparation, L.X.; writing—review and editing, J.S., J.Z., Y.L. (Ying Liu 1), Y.L. (Ying Liu 2), C.J., J.L. and L.X. All authors have read and agreed to the published version of the manuscript.

Funding: This research was funded by the National Natural Science Foundation of China (grant numbers 12004104 and 12204515) and the Young Elite Scientists Sponsorship Program by CAST (grant number 2022QNRC001).

Institutional Review Board Statement: Not applicable.

Informed Consent Statement: Not applicable.

Data Availability Statement: Data are available upon request to the corresponding author.

Conflicts of Interest: The authors declare no conflicts of interest.

References

1. Kamihara, Y.; Watanabe, T.; Hirano, M.; Hosono, H. Iron-based layered superconductor La[$O_{1-x}F_x$]FeAs (x = 0.05–0.12) with T_c = 26 K. *J. Am. Chem. Soc.* **2008**, *130*, 3296. [CrossRef] [PubMed]
2. Bednorz, J.G.; Muller, K.A. Possible high Tc superconductivity in the Ba−La−Cu−O system. *Z. Fur Phys. B Condens. Matter* **1986**, *64*, 189–193. [CrossRef]
3. Rotter, M.; Tegel, M.; Johrendt, D. Superconductivity at 38 K in the iron arsenide ($Ba_{1-x}K_x$)Fe_2As_2. *Phys. Rev. Lett.* **2008**, *101*, 107006. [CrossRef]
4. Sasmal, K.; Lv, B.; Lorenz, B.; Guloy, A.M.; Chen, F.; Xue, Y.Y.; Chu, C.W. Superconducting fe-based compounds ($A_{1-x}Sr_x$)Fe_2As_2 with A = K and Cs with transition temperatures up to 37 K. *Phys. Rev. Lett.* **2008**, *101*, 107007. [CrossRef] [PubMed]
5. Zhao, K.; Liu, Q.Q.; Wang, X.C.; Deng, Z.; Lv, Y.X.; Zhu, J.L.; Li, F.Y.; Jin, C.Q. Superconductivity above 33 K in ($Ca_{1-x}Na_x$)Fe_2As_2. *J. Phys. Condens. Matter* **2010**, *22*, 222203. [CrossRef] [PubMed]
6. Jiang, S.; Xing, H.; Xuan, G.; Wang, C.; Ren, Z.; Feng, C.; Dai, J.; Xu, Z.A.; Cao, G. Superconductivity up to 30 K in the vicinity of the quantum critical point in $BaFe_2(As_{1-x}P_x)_2$. *J. Phys. Condens. Matter* **2009**, *21*, 382203. [CrossRef] [PubMed]
7. Thaler, A.; Ni, N.; Kracher, A.; Yan, J.Q.; Bud'ko, S.L.; Canfield, P.C. Physical and magnetic properties of $Ba(Fe_{1-x}Ru_x)_2As_2$ single crystals. *Phys. Rev. B* **2010**, *82*, 014534. [CrossRef]
8. Sefat, A.S.; Jin, R.Y.; McGuire, M.A.; Sales, B.C.; Singh, D.J.; Mandrus, D. Superconductivity at 22 K in Co-doped $BaFe_2As_2$ crystals. *Phys. Rev. Lett.* **2008**, *101*, 117004. [CrossRef]
9. Li, L.J.; Luo, Y.K.; Wang, Q.B.; Chen, H.; Ren, Z.; Tao, Q.; Li, Y.K.; Lin, X.; He, M.; Zhu, Z.W.; et al. Superconductivity induced by Ni doping in $BaFe_2As_2$ single crystals. *New. J. Phys.* **2009**, *11*, 025008. [CrossRef]
10. Thaler, A.; Hodovanets, H.; Torikachvili, M.S.; Ran, S.; Kracher, A.; Straszheim, W.; Yan, J.Q.; Mun, E.; Canfield, P.C. Physical and magnetic properties of $Ba(Fe_{1-x}Mn_x)_2As_2$ single crystals. *Phys. Rev. B* **2011**, *84*, 144528. [CrossRef]
11. Sefat, A.S.; Singh, D.J.; VanBebber, L.H.; Mozharivskyj, Y.; McGuire, M.A.; Jin, R.; Sales, B.C.; Keppens, V.; Mandrus, D. Absence of superconductivity in hole-doped $BaFe_{2-x}Cr_xAs_2$ single crystals. *Phys. Rev. B* **2009**, *79*, 224524. [CrossRef]
12. Li, X.-G.; Sheng, J.-M.; Tian, C.-K.; Wang, Y.-Y.; Xia, T.-L.; Wang, L.; Ye, F.; Tian, W.; Wang, J.-C.; Liu, J.-J.; et al. Effects of vanadium doping on $BaFe_2As_2$. *EPL* **2018**, *122*, 67006. [CrossRef]
13. Suzuki, H.; Yoshida, T.; Ideta, S.; Shibata, G.; Ishigami, K.; Kadono, T.; Fujimori, A.; Hashimoto, M.; Lu, D.H.; Shen, Z.X.; et al. Absence of superconductivity in the hole-doped Fe pnictide $Ba(Fe_{1-x}Mn_x)_2As_2$: Photoemission and X-ray absorption spectroscopy studies. *Phys. Rev. B* **2013**, *88*, 100501. [CrossRef]
14. Marty, K.; Christianson, A.D.; Wang, C.H.; Matsuda, M.; Cao, H.; VanBebber, L.H.; Zarestky, J.L.; Singh, D.J.; Sefat, A.S.; Lumsden, M.D. Competing magnetic ground states in nonsuperconducting $Ba(Fe_{1-x}Cr_x)_2As_2$ as seen via neutron diffraction. *Phys. Rev. B* **2011**, *83*, 060509. [CrossRef]
15. Sefat, A.S.; Nguyen, G.D.; Parker, D.S.; Fu, M.M.; Zou, Q.; Li, A.-P.; Cao, H.B.; Sanjeewa, L.D.; Li, L.; Gai, Z. Local superconductivity in vanadium iron arsenide. *Phys. Rev. B* **2019**, *100*, 104525. [CrossRef]
16. Konzen, L.M.; Sefat, A.S. Lattice parameters guide superconductivity in iron-arsenides. *J. Phys. Condens. Matter* **2017**, *29*, 083001. [CrossRef]
17. Sundareswari, M.; Jayalakshmi, D.S.; Viswanathan, E. A first principles study on newly proposed (Ca/Sr/Ba)Fe_2Bi_2 compounds with their parent compounds. *Philos. Mag.* **2016**, *96*, 511–523. [CrossRef]
18. Jayalakshmi, D.S.; Sundareswari, M.; Viswanathan, E.; Hemanand, D.; Pranesh, V. Computational study on unconventional superconductivity and mechanical properties of novel antiferrromagnetic (Ca,Sr,Ba)Fe_2Bi_2 compounds. *Int. J. Mod. Phys. B* **2019**, *33*, 1950341. [CrossRef]
19. Vegard, L. Die Konstitution der Mischkristalle und die Raumfüllung der Atome. *Z. Phys.* **1921**, *5*, 17–26. [CrossRef]
20. Kim, J.S.; Blasius, T.D.; Kim, E.G.; Stewart, G.R. Superconductivity in undoped single crystals of $BaFe_2As_2$: Field and current dependence. *J. Phys. Condens. Matter* **2009**, *21*, 342201. [CrossRef]

21. Xiao, H.; Hu, T.; He, S.K.; Shen, B.; Zhang, W.J.; Xu, B.; He, K.F.; Han, J.; Singh, Y.P.; Wen, H.H.; et al. Filamentary superconductivity across the phase diagram of $Ba(Fe,Co)_2As_2$. *Phys. Rev. B* **2012**, *86*, 064521. [CrossRef]
22. Xiao, H.; Hu, T.; Dioguardi, A.P.; apRoberts-Warren, N.; Shockley, A.C.; Crocker, J.; Nisson, D.M.; Viskadourakis, Z.; Tee, X.; Radulov, I.; et al. Evidence for filamentary superconductivity nucleated at antiphase domain walls in antiferromagnetic $CaFe_2As_2$. *Phys. Rev. B* **2012**, *85*, 024530. [CrossRef]
23. Saha, S.R.; Butch, N.P.; Kirshenbaum, K.; Paglione, J.; Zavalij, P.Y. Superconducting and ferromagnetic phases induced by lattice distortions in stoichiometric $SrFe_2As_2$ single crystals. *Phys. Rev. Lett.* **2009**, *103*, 037005. [CrossRef]
24. Zhang, W.; Dai, Y.-M.; Xu, B.; Yang, R.; Liu, J.-Y.; Sui, Q.-T.; Luo, H.-Q.; Zhang, R.; Lu, X.-Y.; Yang, H.; et al. Magnetoresistivity and filamentary superconductivity in nickel-doped $BaFe_2As_2$. *Chin. Phys. B* **2016**, *25*, 047401. [CrossRef]
25. Nguyen, G.D.; Fu, M.; Zou, Q.; Sanjeewa, L.D.; Li, A.P.; Sefat, A.S.; Gai, Z. Nanoscale Superconducting States in the Fe-Based Filamentary Superconductor of Pr-Doped $CaFe_2As_2$. *Nanomaterials* **2021**, *11*, 1019. [CrossRef]
26. Hashimoto, K.K.; Cho, T.; Shibauchi, S.; Kasahara, Y.; Mizukami, R.; Katsumata, Y.; Tsuruhara, T.; Terashima, H.; Ikeda, M.A.; Tanatar, H.; et al. A Sharp Peak of the Zero-Temperature Penetration Depth at Optimal Composition in $BaFe_2(As_{1-x}P_x)_2$. *Science* **2012**, *336*, 1554. [CrossRef]
27. Zhou, R.; Li, Z.; Yang, J.; Sun, D.L.; Lin, C.T.; Zheng, G.-Q. Quantum criticality in electron-doped $BaFe_{2-x}Ni_xAs_2$. *Nat. Commun.* **2013**, *4*, 2265. [CrossRef]
28. Kasahara, S.; Shibauchi, T.; Hashimoto, K.; Nakai, Y.; Ikeda, H.; Terashima, T.; Matsuda, Y. Abrupt recovery of Fermi-liquid transport following the collapse of the c axis in $CaFe_2(As_{1-x}P_x)2$ single crystals. *Phys. Rev. B* **2011**, *83*, 060505. [CrossRef]
29. Werthamer, N.R.; Helfand, E.; Hohenberg, P.C. Temperature and Purity Dependence of the Superconducting Critical Field,Hc2. III. Electron Spin and Spin-Orbit Effects. *Phys. Rev.* **1966**, *147*, 295–302. [CrossRef]
30. Kumar, N.; Nagalakshmi, R.; Kulkarni, R.; Paulose, P.L.; Nigam, A.K.; Dhar, S.K.; Thamizhavel, A. Anisotropic magnetic and superconducting properties of $CaFe_{2-x}Co_xAs_2$(x=0,0.06) single crystals. *Phys. Rev. B* **2009**, *79*, 012504. [CrossRef]
31. Zhu, X.; Yang, H.; Fang, L.; Mu, G.; Wen, H.-H. Upper critical field, Hall effect and magnetoresistance in the iron-based layered superconductor $LaFeAsO_{0.9}F_{0.1-\delta}$. *Supercond. Sci. Technol.* **2008**, *21*, 105001. [CrossRef]
32. Clogston, A.M. Upper Limit for the Critical Field in Hard Superconductors. *Phys. Rev. Lett.* **1962**, *9*, 266–267. [CrossRef]
33. Zhang, G.M.; Su, Y.H.; Lu, Z.Y.; Weng, Z.Y.; Lee, D.H.; Xiang, T. Universal linear-temperature dependence of static magnetic susceptibility in iron pnictides. *EPL* **2009**, *86*, 37006. [CrossRef]
34. Harriger, L.W.; Liu, M.; Luo, H.; Ewings, R.A.; Frost, C.D.; Perring, T.G.; Dai, P. Temperature dependence of the paramagnetic spin excitations in $BaFe_2As_2$. *Phys. Rev. B* **2012**, *86*, 140403. [CrossRef]
35. Allred, J.M.; Taddei, K.M.; Bugaris, D.E.; Avci, S.; Chung, D.Y.; Claus, H.; dela Cruz, C.; Kanatzidis, M.G.; Rosenkranz, S.; Osborn, R.; et al. Coincident structural and magnetic order in $BaFe_2(As_{1-x}P_x)_2$ revealed by high-resolution neutron diffraction. *Phys. Rev. B* **2014**, *90*, 104513. [CrossRef]
36. Hu, D.; Lu, X.; Zhang, W.; Luo, H.; Li, S.; Wang, P.; Chen, G.; Han, F.; Banjara, S.R.; Sapkota, A.; et al. Structural and Magnetic Phase Transitions near Optimal Superconductivity in $BaFe_2(As_{1-x}P_x)_2$. *Phys. Rev. Lett.* **2015**, *114*, 157002. [CrossRef]
37. Sharma, S.; Bharathi, A.; Chandra, S.; Reddy, V.R.; Paulraj, S.; Satya, A.T.; Sastry, V.S.; Gupta, A.; Sundar, C.S. Superconductivity in Ru-substituted polycrystalline $BaFe_{2-x}Ru_xAs_2$. *Phys. Rev. B* **2010**, *81*, 174512. [CrossRef]
38. Sharma, S.; Bharathi, A.; Vinod, K.; Sundar, C.S.; Srihari, V.; Sen, S.; Ghosh, H.; Sinha, A.K.; Deb, S.K. Structural investigations in $BaFe_{2-x}Ru_xAs_2$ as a function of Ru and temperature. *Acta Crystallogr. B Struct. Sci. Cryst. Eng. Mater.* **2015**, *71*, 61–67. [CrossRef]